PERGAMON

Solid State Communications 122 (2002) 317–322

solid state communications

www.elsevier.com/locate/ssc

Stability of $LiMn_2O_4$ and new high temperature phases in air, O_2 and N_2

Vincenzo Massarotti*, Doretta Capsoni, Marcella Bini

Dipartimento di Chimica Fisica "M. Rolla" e CSTE-CNR, Università di Pavia, viale Taramelli 16, 27100 Pavia, Italy

Received 25 January 2002; accepted 8 March 2002 by P. Wachter

Abstract

We investigate the reversible and irreversible transformations, the Li, Mn spinel undergoes under different atmospheres (air, O_2, and N_2) when heated up to 1050 °C. In air and O_2, a substantial reversible cation exchange occurs. For $T \geq 800$ °C, Mn^{2+} ions substitute Li^+ at the tetrahedral (8a) position, and Li^+ shifts to interstitial octahedral (16c) site. Charge balance is achieved by a decrease in the Mn^{3+} fraction, which is partially reduced to Mn^{2+} in the regular octahedral (16d) site, according to the charge distribution $(Li^+_{1-2y}Mn^{2+}_{2y})_{8a}[Li^+_{3y}]_{16c}[Mn^{2+}_{5y}Mn^{3+}_{1-5y}Mn^{4+}_{1}]_{16d}O_4$ (y increases with T). Under N_2 flow, a first decomposition occurs between 600 and 800 °C and yields Mn_3O_4, orthorhombic $LiMnO_2$ and O_2. A minor O_2 release occurs when heating above 900 °C, which is accompanied by the transformation of o-$LiMnO_2$ into a cubic $Li_xMn_{1-x}O$ solid solution ($x \leq 0.5$), consistent with a decrease in the average oxidation state of Mn ions. This cubic phase is stable at high temperature and decomposes upon cooling ($T \leq 800$ °C) leaving just the Mn_3O_4 and o-$LiMnO_2$ phases. © 2002 Published by Elsevier Science Ltd.

PACS: 61.12.Ld

Keywords: C. X-ray powder diffraction; C. Point defects; D. Phase transition; D. Thermal decomposition

1. Introduction

The use of $LiMn_2O_4$ as an electrode for rechargeable lithium ion cells was proposed more than 20 years ago [1], and this material was extensively characterised a decade later [2–5]. The current interest in the compound is still more, and is focussing upon new routes of chemical and electrochemical synthesis for both stoichiometric and nonstoichiometric spinel phases. Composition-valence 'phase diagrams' have been proposed mainly on the basis of mass variation, X-ray powder diffraction (XRD) data [5–7], and the general formula $Li_{1+y}Mn_{2-y}O_4$.

At low oxygen pressures, a deficit of oxygen occurs in $LiMn_2O_{4-\delta}$, where δ was determined as a function of temperature by thermogravimetry (TG) and chemical titration [8,9]. Furthermore, in the range $620 < T < 1100$ °C, the oxygen loss and the enthalpy change (from DSC runs) quantitatively agree with the decomposition of the spinel to give Mn_3O_4 and $LiMnO_2$ [10,11]. Evidence for $LiMnO_2$ phase formation in air comes from in situ XRD measurements of $LiMn_2O_4$ in the T-range 960–1080 °C [5]: $LiMnO_2$ and Li_2MnO_3 coexist. More recently, the role of different preparation routes upon phase transformation and stability has been demonstrated [12,13]. We need a deep understanding of the stability of the spinel phase in order to plan synthesis and sinterisation processes that achieve final composition and structure which are optimal for electrochemistry and catalysis.

For a better understanding of the mechanisms of thermal decomposition of the spinel phase, we planned a study of the stoichiometric $LiMn_2O_4$ as a function of oxygen partial pressure, in the temperature range 25–1050 °C, by TG and in situ XRD measurements.

2. Experimental

A stoichiometric $LiMn_2O_4$ sample has been prepared by adding Li_2CO_3 and Mn(III)acetylacetonate in proper

* Corresponding author. Fax: +39-382-507575.
E-mail address: vimas@chifis.unipv.it (V. Massarotti).

0038-1098/02/$ - see front matter © 2002 Published by Elsevier Science Ltd.
PII: S0038-1098(02)00149-7

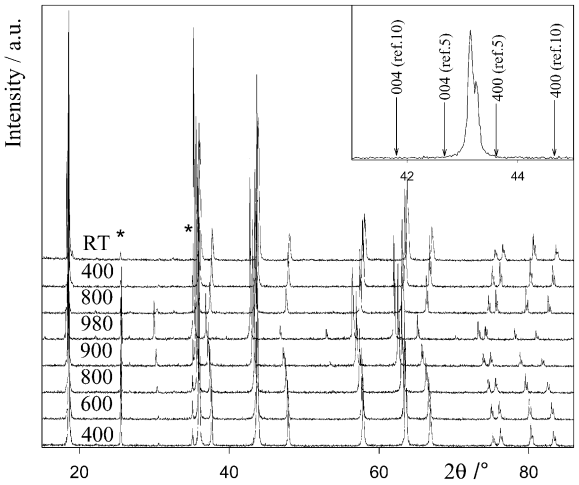

Fig. 1. XRD patterns of a stoichiometric spinel during a heating/cooling cycle in air. The reflections marked with stars are due to the alumina sample holder. In the inset, the 400 cubic reflection is shown and compared with theoretical positions for the tetragonal cells reported in literature [5,10].

amount to boiling propionic acid [14]. After solvent evaporation and drying in vacuum, the powder was treated in air at 500 °C for 18 h, then heated for 18 h at 900 °C (heating and cooling rate of 5 °C/min).

The XRD patterns have been collected with a Bruker D5005 diffractometer (Bragg–Brentano geometry, graphite monochromator, Cu Kα radiation). The high temperature patterns were obtained with an HTK1200 Anton Paar polythermal attachment with alumina sample holder. The atmosphere was N_2, O_2 (flow rate 5 l/h), or air. The patterns have been collected up to 980 °C in O_2 and air, and up to 1050 °C in N_2. Heating and cooling rate was 0.08 °C/s; the measurements have been performed in the $13 \leq 2\theta \leq 93°$ angular range.

TG measurements were run by means of a 2950 TGA (TA Instruments) controlled by a TA 5000 system (flows and heating cycles as for XRD).

The XRD data were analysed by Rietveld method [15], based on the minimisation of the residual:

$$M = \sum w_i (y_{o,i} - y_{c,i})^2 \quad (1)$$

where $y_{o,i}$ and $y_{c,i}$ are the observed and calculated intensities at point i of the diffraction pattern and w_i the pertinent statistical weight. For the case of a system containing p crystalline phases, $y_{c,i}$ can be written as

$$y_{c,i} = y_{b,i} + \sum_p K_p \sum_h m_{h,p} L_{h,p} |F_{h,p}|^2 G_{h,p,i} A_{h,p,i} \quad (2)$$

where $y_{b,i}$ is the background intensity contribution, K_p the scale factor related to the mass percentage of the same p phase, $m_{h,p}$ the multiplicity of the reflection, $L_{h,p}$ the Lorentz-polarisation factor, $F_{h,p}$ the structure factor, $G_{h,p,i}$ the peak profile function (Pearson VII), $A_{h,p,i}$ the peak

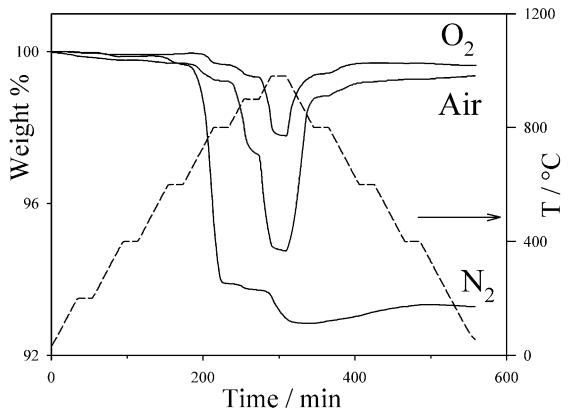

Fig. 2. TG measurements of $LiMn_2O_4$ in air, O_2 and N_2. Dashed line represents the thermal cycle.

asymmetry function. For each phase, all the h reflections contributing to the diffracted intensity at point i are considered. The parameters of the multiphase model were refined using the FULLPROF program [16] and a procedure described elsewhere [17]. The relative abundance of phases and occupancies of cation sites have been estimated and the reliability of the results have been evaluated by means of the discrepancy factor R_{wp} and χ^2 [15,16].

3. Results

3.1. Measurements in air or in O_2 flow

The XRD patterns collected during a heating/cooling cycle in air are shown in Fig. 1. Similar patterns are obtained during the same cycle in oxygen. In both sets, the cubic $LiMn_2O_4$ spinel is the only phase detected up to 980 °C. No evidence for the formation of tetragonal spinel phases at $780 < T < 915$ °C [5,10] have been found (inset of Fig. 1).

The intensity of the 220 spinel reflection (at $2\vartheta \approx 30°$) changes above 600 °C. This phenomenon is related to a modified cationic distribution, with Mn ions that, at high temperatures, begin to occupy the Li^+ tetrahedral site [5]. This displacement is also related to an increase in the very weak 422 and 620 reflections (at $2\vartheta \approx 54$ and 72°, respectively, see Fig. 1). Occupancy of the 8a site by Mn is more pronounced in air than in oxygen atmosphere, which suggests that the change in cation distribution is driven by a release of O_2. In fact, TG measurements (Fig. 2) confirm that the weight loss upon heating is higher in air than in O_2. Both TG and XRD measurements suggest that the process is reversible.

The Rietveld structural and profile refinement has been performed assuming a cubic spinel phase. For $T > 600$ °C, a modified cubic spinel model was applied where a fraction of Mn is placed at the 8a lattice site and a corresponding amount of Li is displaced from 8a site to the neighbouring

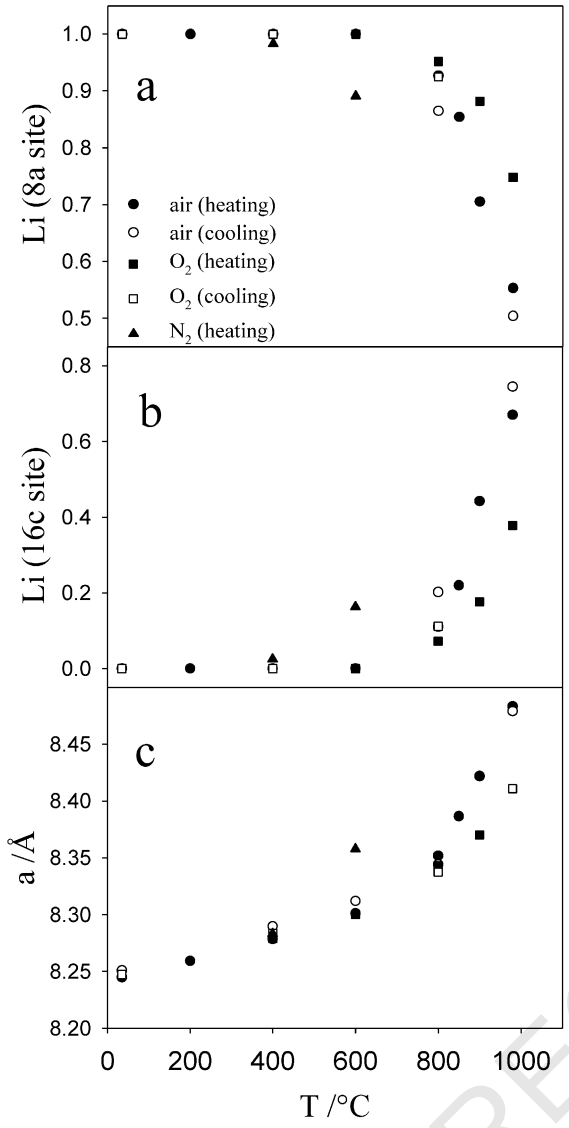

Fig. 3. Fractional site occupancy of lithium in the 8a site (a), 16c site (b), and lattice parameters (c) of cubic spinel phase during thermal cycles in different atmospheres as a function of temperature.

interstitial 16c site. The closeness of the 8a and 16c sites, whose polyhedra share a face, may justify lithium shift. This Li^+ insertion/migration in a 16c site is strictly related to the transformation occurring in charge/discharge electrochemical processes [18,19]. Some trials have been carried out using an inverse spinel model, proposed for quenched samples [10]: we could not obtain satisfactory fits, in agreement with the results obtained by Thackeray et al. [5]. This may imply that the 16d site is fully occupied by Mn ions even for $T \geq 800$ °C.

The Mn amount on 8a site (Mn plus Li occupancy constrained to 100%) increases with temperature. Upon cooling this process is reversible, with some hysteresis. The

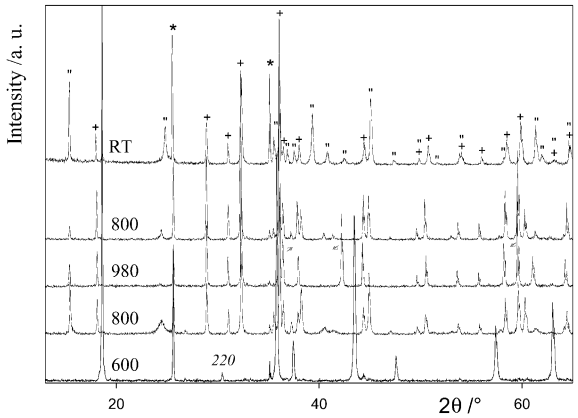

Fig. 4. Most significant XRD patterns obtained in a heating/cooling cycle under N_2. The symbols are pertinent to the phases: Al_2O_3 (*), Mn_3O_4 (+), *o*-$LiMnO_2$ ($''$) and $Li_xMn_{1-x}O$ (→).

Li occupancy of the 8a and 16c sites (Li 16c constrained so that 1:2 Li/Mn ratio is achieved), as obtained by fitting the modified spinel model, is shown in Fig. 3(a) and (b) as a function of *T*. The *a* lattice parameter of the spinel has been evaluated for both air and O_2 experiments, and its dependence on *T* is shown in Fig. 3(c). Satisfactory χ^2 (1.30–1.56) and R_{wp} (22.5–26.2 %) values were obtained.

3.2. Measurements in N_2 flow

The most significant XRD patterns are shown in Fig. 4. The spinel phase is stable up to 600 °C and it does not show any evidence of change in cation distribution for $T \leq 400$ °C. At 600 °C, the intensity of the 220 peak (Fig. 4) increases: our refinement yields about 10% of 8a sites occupied by Mn, the same amount attained at 800 °C in air (Fig. 3(a) and (b)). Between 600 and 800 °C, $LiMn_2O_4$ completely transforms into Mn_3O_4 and orthorhombic $LiMnO_2$ phases. A weight loss of ~6% is observed (Fig. 2). At 980 °C, we have the 100 reflection of the *o*-$LiMnO_2$ phase ($2\theta \sim 15.5°$) along with a new set of peaks (arrows in Fig. 4), attributed to a cubic lithium manganese oxide phase with a MnO structure. This phase may be produced through a mechanochemical process [20], but was not otherwise observed before. Upon cooling, this phase reverts again to an orthorhombic phase, which is stable down to room temperature and coexists with Mn_3O_4.

An additional set of data was collected during a heating/cooling cycle at 930, 960, 1000, 1050, 800, and 35 °C. At 930 °C, the pattern is fully explained by Mn_3O_4 and *o*-$LiMnO_2$. At 960 °C, the orthorhombic to cubic transformation is underway and both phases are present. The 980 °C pattern of the previous set had only the 100 reflection of the orthorhombic phase, but not the other reflections of *o*-$LiMnO_2$. This fact suggests that, at 980 °C, the orthorhombic to cubic transformation completes in about 30 min. The *o*-$LiMnO_2$ is not seen in the patterns with

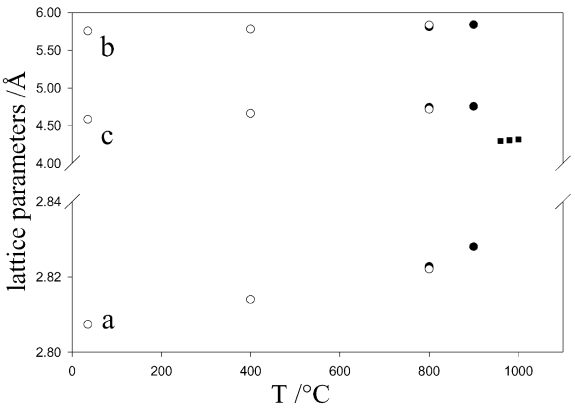

Fig. 5. Lattice parameters of o-$LiMnO_2$ (full circles, heating; open circles, cooling) and cubic $Li_xMn_{1-x}O$ (squares) phases from measurements performed under N_2.

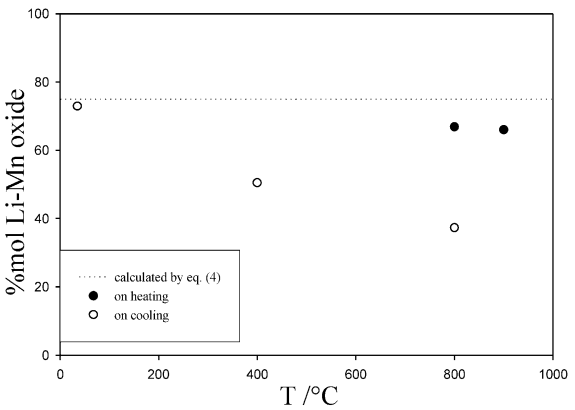

Fig. 6. Mol percentage of Li–Mn oxide (o-$LiMnO_2$ or cubic $Li_xMn_{1-x}O$) in comparison with the expected value (Eq. (4)) as a function of temperature for samples treated in N_2 flow.

$T \geq 1000$ °C. The patterns obtained during cooling are somehow different from those of the previous set, and the differences are believed to be caused by the harder annealing. At 800 °C, in addition to Mn_3O_4, only the cubic form is present in the second set, and not o-$LiMnO_2$. At 35 °C, we now have a cubic MnO phase in addition to the o-$LiMnO_2$ and Mn_3O_4.

The lattice parameters, as given by Rietveld refinement, are plotted vs. T in Fig. 3(c) (spinel phase) and Fig. 5 (o-$LiMnO_2$ and cubic lithium manganese oxide). The fractions (in mol%) of Li–Mn oxide are shown in Fig. 6 as a function of temperature.

4. Discussion

The spinel phase is stable up to 980 °C in air or O_2 atmospheres, whereas an irreversible decomposition takes place between 600 and 800 °C in N_2. The lattice expansion increases faster in air than in oxygen for $T > 800$ °C (Fig. 3(c)), which agrees with the higher a values obtained in quenched samples relative to the slowly cooled ones [10]. The Li occupancy of the 8a site displays a remarkable dependence on the oxygen partial pressure above 800 °C, and decreases with decreasing $p(O_2)$ (Fig. 3(a)). However, the electronic density of the site increases, as signalled by the higher intensity of the 220 reflection (Fig. 1), meaning that lithium is substituted by Mn ion. The spinel lattice is preserved (inset of Fig. 1) and oxygen vacancies in the anionic sublattice should not be taken into account in the explored $p(O_2)$ range [9]. We have no evidence by Rietveld refinement of Mn substitution by Li ions at 16d site, and we should rule out even the minor ($\sim$10%) inversion of spinel suggested by Tarascon et al. [10]. After the thermal cycle, we obtained the same spinel phase as initial one, suggesting the preservation of 1:2 Li/Mn ratio. Therefore, a model is suggested, in which the Li^+ ion can be inserted into the octahedral 16c site, contributing to the overall charge balance according to the following equilibrium, valid for $y \leq 0.2$

$$(1+y)LiMn_2O_4 \leftrightarrows \left(Li^+_{1-2y}Mn^{2+}_{2y}\right)_{8a}\left[Li^+_{3y}\right]_{16c}\left[Mn^{2+}_{5y}Mn^{3+}_{1-5y}Mn^{4+}_{1}\right]_{16d}O_4 + 2yO_2 \quad (3)$$

The presence of Mn^{2+} at 8a site was suggested also by Thackeray et al. [5]. If we assumed only Mn^{3+} and Mn^{4+}(and not Mn^{2+}) at the 16d site, a different kind of charge and mass balance should have been obtained; in particular, we should have had a significant increase in Mn^{3+} that would contribute to the Jahn–Teller distortion of the spinel structure. Such a tetragonal distortion previously reported [5,10,12,21] has never been observed in our measurements (inset of Fig. 1).

With increasing temperature, the y value increases, the mean valence of Mn decreases and oxygen is released, in agreement with the TG results in Fig. 2. At 980 °C in air the mean valence of Mn is 2.83, while the initial value was 3.5 and that of Mn_3O_4 (tetragonal spinel) is 2.66. This process is reversible, and the high temperature form is re-oxidised, upon cooling, back to the stoichiometric $LiMn_2O_4$. In the high temperature 'cation-rich' phase, Li^+ ion can occupy up to 30% of the interstitial 16c site. Theoretical calculation of defect formation energy in $LiMn_2O_4$ at rt shows that Li Frenkel defect (1.65 eV) is strongly preferred with respect to other possible ones [22]. It is well known that the 16c site is involved also for the 'Li-rich' $Li_2Mn_2O_4$ compound, which contains only Mn^{3+} in a tetragonal structure [7,19]. Instead, the present cation-rich spinel may have lower average valence because of the presence of Mn^{2+} (Eq. (3)). Thus, at high temperatures, the Mn^{3+} decreases and the cubic symmetry of the site is preserved. In air, the cation distribution over the spinel 8a site is a function of temperature and basically reversible; at 600 °C a full 8a occupancy by Li is observed (both upon heating and

cooling), while at 800 °C is 0.93(1) when heating and 0.87(2) when cooling. The associated mass variation, due to oxygen release according to Eq. (3), would be 1.2% from 600 to 800 °C, in good agreement with the TG data (Fig. 2).

Our slow thermal cycling yields results somehow different from those obtained with samples quenched in air [10] or directly synthesised at high temperature [5]. For samples quenched from $T > 800$ °C, it seems that fast cooling inhibited the equilibrium with O_2. For the in situ high temperature measurements [5] the differences may be due to the special experimental setting and the very thin (sprayed) sample analysed. Surface reactions may have occurred at $T \approx 715$ °C with the formation of a Li_2MnO_3 phase, which get transformed at higher temperatures. Different synthesis routes may influence the high temperature stability of the spinel. In effect, different structures and/or microstructures can be stable at the same annealing temperature, depending on sample preparation [12,23]. In fact, the sample synthesised via sol–gel has morphology and crystallite size different from those of a sample obtained by solid state reaction [11,23].

Under a N_2 flow, a modest release of oxygen occurs between 400 and 600 °C indicating that cation mixing has already begun (Fig. 3(a) and (b)). This fact agrees with a higher value of the a parameter for the cubic spinel at 600 °C, which is attained only at 800 °C in air or under O_2 (Fig. 3c). In addition, between 600 and 800 °C, the following reaction occurs:

$$3LiMn_2O_4 \rightarrow Mn_3O_4 + 3LiMnO_2 + O_2 \quad (4)$$

The amount of $LiMnO_2$ (Fig. 6) is very similar to the value obtained from refinement, assuming the proper multiphase structural model. The complete reaction implies about 6% of oxygen loss, in agreement with the result of TG measurement between 600 and 800 °C (Fig. 2). Mn_3O_4 is stable over the explored temperature range while $LiMnO_2$ maintains its orthorhombic form only below 930 °C. At higher temperatures ($960 \leq T \leq 1050$ °C), the cubic solid solution $Li_xMn_{1-x}O$ with $x \leq 0.5$ and Mn oxidation state $(2 - x)/(1 - x)$ is created according to the reaction:

$$(1 - x)LiMnO_2 \rightarrow Li_xMn_{1-x}O + 0.5(1 - 2x)Li_2O + 0.25(1 - 2x)O_2 \quad (5)$$

The oxygen released is lost in the N_2 flow and no longer available for the reverse reaction when cooling. Assuming that the overall weight loss, of about 1.6% (Fig. 2), between ≈900 and 980 °C is due to release of O_2, we would have $x \approx 0.45$. The Li_2O phase formed (about 3% by weight), was not identified by diffraction, probably because it gives an amorphous segregation. On cooling, the cubic solid solution disappears below 800 °C and o-$LiMnO_2$ is observed. The transformation could follow the reaction:

$$Li_xMn_{1-x}O \rightarrow (5x - 2)LiMnO_2 + (1 - 2x)Mn_3O_4 + (1 - 2x)Li_2O \quad (6)$$

At rt, we finally observe the proportion of phases (Fig. 6) predicted by Eq. (4), confirming that no Li loss occurred during the thermal process. The underestimation of o-$LiMnO_2$ for 800 °C ≥ T ≥ rt (Fig. 6) could be related to a delayed crystallisation of the orthorhombic form for kinetic reasons. When the sample has been annealed a long time (more than 10 h) at $T > 1000$ °C, the XRD patterns obtained during cooling show the presence of the cubic form below 800 °C. At rt MnO, Mn_3O_4 and o-$LiMnO_2$ were detected, according to the stabilisation of a lower Mn mean oxidation state.

5. Conclusions

In the spinel phase we observed that the 8a site and an interstitial 16c site are involved in reversible changes of ionic distribution occurring at high temperatures in air or O_2. Between 800 and 980 °C, lithium progressively occupies an interstitial site and a substantial change in charge distribution involving the Mn ions occurs according to Eq. (3). The average oxidation state of Mn decreases with increasing temperature but, upon cooling, the reverse reaction takes place with an O_2 uptake which occurs down to 600 °C, as confirmed by TG measurements.

Under N_2 flow, more complex and irreversible reactions take place. The first decomposition step of spinel phase is accomplished between 600 and 800 °C according to Eq. (4): oxygen loss accompanies the formation of o-$LiMnO_2$ and Mn_3O_4 phases. The second step pertains to the transformation of o-$LiMnO_2$ into $Li_xMn_{1-x}O$ cubic solid solution, according to Eq. (5). At each temperature, an equilibrium is attained and the phases observed in the diffraction patterns depend on both temperature and time of the annealing.

All these reactions are characteristic gas/solid processes: surfaces and grain boundaries are certainly involved along with residual segregated materials in their crystalline or amorphous state. Thus, preparation and morphology of the precursor material play a fundamental role in the outcome of the sintering procedure and the final properties (electrochemical or catalytic) of the lithium manganese spinel.

This work provides a wealth of new information about interface reactions and cation distribution over the spinel sites as a function of oxygen partial pressure. A number of transformations occur between 600 and 800 °C, a temperature range where the material is usually synthesised and where it undergoes sintering processes. We argue that a better knowledge of the stability of spinel and its reactivity with oxygen is fundamental to achieve the performances needed for technological exploitation of the compound.

Acknowledgments

The authors gratefully acknowledge Prof. M. Villa for helpful discussion and Dr C. Tomasi for having carried out the TG measurements. This work has been partially supported by 'Consorzio per i Sistemi a Grande Interfase' (CSGI) and Progetto Finalizzato MSTA II of Italian CNR.

References

[1] K. Mizushima, P.C. Jones, P.J. Wiseman, J.B. Goodenough, Mater. Res. Bull. 15 (1980) 783.
[2] T. Ohzuku, M. Kitagawa, T. Hirai, J. Electrochem. Soc. 137 (1990) 769.
[3] J.M. Tarascon, D. Guyomard, J. Electrochem. Soc. 138 (1991) 2864.
[4] J.M. Tarascon, D. Guyomard, Electrochim. Acta 38 (1993) 1221.
[5] M.M. Thackeray, M.F. Mansuetto, D.W. Dees, D.R. Vissers, Mater. Res. Bull. 31 (1996) 133.
[6] F. Le Cras, P. Strobel, M. Anne, D. Bloch, J.B. Soupart, J.-C. Rousche, Eur. J. Solid State Inorg. Chem. 33 (1996) 67.
[7] P. Strobel, F. Le Cras, M. Anne, J. Solid State Chem. 124 (1996) 83.
[8] J. Sugiyama, T. Atsumi, T. Hioki, S. Noda, N. Kamegashir, J. Alloys Compd 235 (1996) 163.
[9] M. Hosoya, H. Ikuta, T. Uchida, M. Wakihara, J. Electrochem. Soc. 144 (1997) L52.
[10] J.M. Tarascon, W.R. McKinnon, F. Coowar, T.N. Bowmer, G. Amatucci, D. Guyomard, J. Electrochem. Soc. 141 (1994) 1421.
[11] V. Massarotti, M. Bini, D. Capsoni, Z. Naturforsch. 51a (1996) 267.
[12] Y.M. Hon, K.Z. Fung, M.H. Hon, J. Ceram. Soc. Jpn 108 (2000) 462.
[13] M. Gorova, E. Zhecheva, Solid State Ionics 135 (2000) 223.
[14] L. Hernan, J. Morales, L. Sanchez, J. Santos, Solid State Ionics 104 (1997) 205.
[15] H.M. Rietveld, J. Appl. Crystallogr. 2 (1969) 65.
[16] J. Rodriguez-Carvajal, Physica B 192 (1993) 55.
[17] V. Massarotti, M. Bini, D. Capsoni, A. Altomare, A.G.G. Moliterni, J. Appl. Crystallogr. 30 (1997) 123.
[18] H. Berg, K. Goransson, B. Nolang, J.O. Thomas, J. Mater. Chem. 10 (2000) 1437.
[19] W.I.F. David, M.M. Thackeray, L.A. De Picciotto, J.B. Goodenough, J. Solid State Chem. 67 (1987) 316.
[20] M.N. Obrovac, O. Mao, J.R. Dahn, Solid State Ionics 112 (1998) 9.
[21] A. Yamada, K. Miura, K. Hinokuma, M. Tanaka, J. Electrochem. Soc. 142 (1995) 2149.
[22] B. Ammundsen, J. Rozière, M.S. Islam, J. Phys. Chem. B 101 (1997) 8156.
[23] V. Massarotti, D. Capsoni, M. Bini, G. Chiodelli, C.B. Azzoni, M.C. Mozzati, A. Paleari, J. Solid State Chem. 147 (1999) 509.